Universidad de La Laguna

APPLICATION OF 3D PRINTING TO OPTICAL TEMPERATURE SENSORS

Department of Physics, University of La Laguna
San Cristóbal de La Laguna
Santa Cruz de Tenerife, Canarias, España

DEGREE IN PHYSICS

Author:
Almudena Díaz Serrano
Tutors:
Inocencio Rafael Martín Benenzuela
Fernando Rivera López

2024

Contents

Abstract

Luminescence-based optical thermal sensors have been a true revolution in the scientific and industrial field, due to their application in micro- and nano-scale systems and their high sensitivity. The use of 3D printing technology to implement this type of sensors opens the framework for a wide range of industrial applications, creating cheap, efficient and non-invasive thermal optical sensors.

In this work, the fabrication of a thermal sensor in the shape of a hollow tube, doped with an active material is presented. For this purpose, we will study the emission of a fluoroindate glass doped with lanthanide ions, erbium and ytterbium, in order to analyse its viability as an active material for the optical temperature sensor. This sensor will be based on the *LIR technique*, which uses the thermal dependence of thermally coupled levels (TCLs) to find the ratio of emission intensities with increasing temperature. In order to achieve this, the emission bands corresponding to the $^2H_{11/2} \rightarrow^4 I_{15/2}$ and $^4S_{3/2} \rightarrow^4 I_{15/2}$ transitions were used, which emit at wavelengths around 525 and 550 nm, respectively. The temperature range considered was from room temperature 296.8 K to 376.3 K. In addition, essential parameters such as sensitivity and temperature uncertainty were obtained to compare its performance with other similar sensors.

Next, the design and 3D printing of the tube here proposed is detailed. The printing parameters used are indicated, in addition to describing the steps followed for the design of the part, including the different alternatives proposed. The idea is to dope the tube in a durable, cheap and simple way. The inner walls of the tube were covered with an homogeneous mixture of a resin and the active material.

Finally, we will present and discuss the results obtained by measuring the temperature of the tube with the *LIR technique* while a certain liquid flows through it. Three types of measurements were performed, one to check the temperature inside the tube as the temperature of the thermal bath increased, one to analyse the temperature difference at the beginning and at the end of the tube and finally some measurements to obtain the standard deviations of the temperature. Additionally, the possible implications of the results will be discussed and a series of future projects that continue the line of work here developed will be proposed.

Resumen

Los sensores térmicos ópticos basados en luminiscencia han supuesto una auténtica revolución en el campo científico e industrial, debido a su aplicación en sistemas de micro y nano escala y a su alta sensibilidad. El uso de la tecnología de impresión 3D para la implementación de este tipo de sensores abre el marco a un amplio abanico de aplicaciones industriales, creando sensores ópticos térmicos baratos, eficientes y no invasivos.

En este trabajo se propone la fabricación de un sensor térmico en forma de tubo hueco, dopado con un material activo. Para ello, se estudiará la emisión de un vidrio de fluoroindato dopado con iones lantánidos, erbio e iterbio, con el fin de analizar su viabilidad como material activo para el sensor óptico de temperatura. Este sensor se basará en la *técnica LIR*, que utiliza la dependencia térmica de los niveles térmicamente acoplados para hallar la relación entre las intensidades de emisión con el aumento de la temperatura. Para ello, se han utilizado las bandas de emisión correspondientes a las transiciones ${}^2H_{11/2} \rightarrow {}^4 I_{15/2}$ y ${}^4S_{3/2} \rightarrow {}^4 I_{15/2}$, que emiten a longitudes de onda en torno a 525 y 550 nm, respectivamente. El rango de temperatura considerado fue desde la temperatura ambiente 296.8 K hasta 376.3 K. Además, se obtuvieron parámetros esenciales como la sensibilidad y la incertidumbre de temperatura para comparar su rendimiento con el de otros sensores similares.

A continuación, se detalla el diseño y la impresión 3D del tubo aquí propuesto. Se indican los parámetros de impresión utilizados, además de describir los pasos seguidos para el diseño de la pieza, incluyendo las diferentes alternativas propuestas. La idea es dopar el tubo de una forma duradera, barata y sencilla. Las paredes interiores del tubo se recubrieron con una mezcla homogénea de una resina y el material opticamente activo.

Por último, presentaremos y discutiremos los resultados obtenidos midiendo la temperatura del tubo con la *técnica LIR* mientras un determinado líquido fluye a través de él. Se realizaron tres tipos de medidas, una para comprobar la temperatura en el interior del tubo a medida que aumentaba la temperatura del baño térmico, otra para analizar la diferencia de temperatura al principio y al final del tubo y finalmente unas medidas para obtener las desviaciones estándar de la temperatura. Además, se discutirán las posibles implicaciones de los resultados y se propondrán una serie de proyectos futuros que continúen la línea de trabajo aquí desarrollada.

Chapter 1

Introduction

Resumen

En este capítulo se presentarán los conceptos y motivaciones principales detrás de este trabajo, destacando la importancia de la utilización de materiales luminiscentes como sensores ópticos y su amplio uso en la industria. Se analizará la posible combinación de métodos innovadores como impresión 3D y el uso de lantánidos como sensores ópticos. Concretamente se cubrirá una pieza 3D (un tubo hueco) con una mezcla de resina y un medio opticamente activo. Se propone como posible aplicación industrial su utilización como sensor óptico de temperatura. Posteriormente, se explicarán los fundamentos teóricos en los que se sustenta este trabajo. Explicaremos de manera detallada el funcionamiento de la técnica *Luminescence Intensity Ratio (LIR)* empleada para caracterizar la muestra como un sensor térmico óptico. Introduciremos parámetros clave que determinan el buen funcionamiento de un sensor térmico óptico: sensibilidad relativa e incertidumbre de la temperatura. Finalmente, se detallará el proceso de *Upconversion* mediante el cual los iones lantánidos, Er^{3+} e Yb^{3+}, usados como agentes sensitivos, emiten en ciertas longitudes de onda tras ser excitados.

1.1 Interest in measuring physical parameters

In the rapidly expanding modern industry, effective, inexpensive and reliable measurement of physical parameters is essential for numerous medical, scientific and industrial applications. Among parameters such as pressure, humidity, or volume, temperature (T) stands out as a fundamental physical parameter, due to its critical role in determining the state of natural and artificial systems. It is therefore not surprising that the scientific community has placed emphasis on the search for reliable temperature sensors.

In this context, optical temperature sensors have emerged as a promising alternative due to their advantages over conventional temperature sensors, as they provide higher sensitivity, immunity from electromagnetic interference and ease of working at nanometric scales [1].

In the case of traditional sensors that measure by contact, it must be taken into account that the contact between the sensor and the surface of the object can cause temperature exchange, thus altering the measurements. This phenomenon becomes especially relevant in small systems, where the size of the object to be measured is smaller than the sensor head [2]. Therefore, the ability to measure temperature non-invasively without altering the chemical and physical composition is crucial, especially on microscales. This feature allows for more reliable and reproducible outcomes, avoiding potential interferences that could alter the possible results. In scientific areas such as biomedicine, it is essential to be able not to modify the biological system while measuring its temperature. With this aim, multiples researchers are focusing on non-contact thermometry, with luminescent thermometers emerging as a versatile and accurate technique [3][4].

Luminescent thermometers are based on the thermal dependence of luminescent phosphors [5]. These will undergo changes in their luminescent emission spectra as the temperature varies, altering in band shape, peak intensity and lifetime, among other factors. This is due to the temperature-dependent nature of some energy properties of electronic states. Organic dyes, lanthanide ions and quantum dots (QD) are just a few types of luminescent temperature sensors that have been widely used. In this study, we will focus on the use of lanthanide ions (Ln^{3+}) as a medium to develop our optical thermal sensor. Compared with other types of luminescent sensors, materials doped with lanthanide ions present important advantages in terms of high spatial resolution, photostability and can be synthetized by relatively inexpensive methods [6]. One of the most prominent advantages of using lanthanides in luminescent thermometry is their high spatial resolution. This feature allows such sensors to take measurements when spatial resolution decreases to nano scale, where traditional methods are inadequate [7].

Within the lanthanide group, ytterbium ions (Yb^{3+}) are highly efficient at absorbing photons at 980 nm. Er^{3+}, on the other hand, with its multiple energy levels, is excited by the energy transfer of ytterbium. This causes the emission of higher energy photons, a phenomenon known as upconversion. As a consequence, erbium and ytterbium are energetically compatible, allowing efficient energy transfer to occur. Therefore, these ions are particularly effective for our study as optical sensors, due to their high sensitivity [8]. For that reason, we will work with erbium and ytterbium in a glass fluorindate matrix during our project.

1.2 3D printing

In this framework of innovative techniques as solutions to new challenges in the industry, additive manufacturing (AM), also known as 3D printing, has revolutionized the manufacturing sector, changing the means by which products are designed, developed and assembled. In just 40 years since its creation, 3D technology has managed to position itself as a leading technology by offering an inexpensive, fast and simple alternative to traditional additive manufacturing technologies. This technique is based on the creation of three-dimensional objects by superimposing successive layers of material. These materials cover a wide range

of possibilities, using Polylactic Acid (PLA), which is a biodegradable plastic, stainless steel or resins [9].

The versatility AM provides in different fields, solving the drawbacks of other technologies, offer the possibility of creating parts easily and autonomously. For example, the introduction of metal AM processes such as powder bed fusion (PBF) or laser metal deposition (LMD) has made it possible in the aerospace and automotive industries to create and implement parts that were previously unfeasible by traditional formative, subtractive manufacturing or injection moulding. Parts with undercuts and blind holes were once virtually impossible to create using traditional injection moulding methods, whereas for 3D printers this is no longer a challenge [10].

In fields such as materials research, 3D printing has made a substantial impact. The use of different chemical compositions in both the filament and the resins used to create 3D parts allows the manipulation of the physicochemical characteristics of these pieces. Furthermore, doping can be used to modify the properties and improve the capabilities according to the purpose for which the piece in question has been designed, to enhance its insulating, mechanical, thermal, or optical properties, among other aspects [11][12]. As a result, the material by which 3D parts are created has acquired a very important role, opening a wide range of possibilities. Depending on the type of 3D printer, a variety of materials can be used for printing, such as Polylactic Acid (PLA), due to its versatility. Moreover, detecting temperature with optically active ions is one of the most prominent potential uses in which 3D technology can take part in. Being able to use resin as an application medium to add these compounds implies a relatively inexpensive, simple and durable way to dope any type of piece, as long as it can be printed in 3D. Within this enormous list of advances that have been discussed, in this project we are going to use PLA for the printing of the piece and resin as a medium to cover the tube with luminescent materials.

Despite the novelty of this technique, there are reported cases of industrial applications of 3D printed pieces with luminescent material used as thermal optical sensors. These materials have been implemented in pieces such as 3D printed polymers or 3D printed gears [13][14]. In this work, a hollow tube will be proposed as our doped 3D piece. The aim of this innovative approach is to be able to analyse the temperature of a liquid flowing through the tube by studying its luminescence emission.

1.3 Aim of the study

The objectives and motivations for this work will be discussed in this section. The main objective of this project was to create a tube as a optical thermal sensor based on the *LIR* technique. For this purpose, the next steps need to be done:

- Measurement and study of the upconversion emission spectra of a fluorindate glass doped with erbium and ytterbium as a function of temperature.

- Obtain by using the *LIR technique* a relation between the intensity ratio and the temperature, in order to characterise the sample as an optical thermal sensor.
- Calculation and acquisition of the relative sensitivity and temperature uncertainty as crucial parameters for the comparison with other luminescence based optical thermal sensors.
- Creation of a 3D part in a tubular shape, covered with a mixture of resin and fluorindate glass doped with erbium and ytterbium.
- Analysis of the tube performance as an optical thermal sensor. This analysis is carried out generating a constant flow of water in the tube and heating the water up to a certain temperature.
- Measurements of the temperature difference at the beginning and at the end of the tube.
- Study of the repeatability of the measurements to determine the reliability of the sensor.

1.4 Theoretical Background

1.4.1 Luminescence intensity ratio technique (LIR)

As a means to calibrate the temperature sensor, the luminescence intensity ratio (*LIR*) technique was used. This technique entails the recording of the luminescence intensities coming from two energy levels, such as ${}^2H_{11/2}$ and ${}^4S_{3/2}$ levels of Er^{3+}, as a function of the physical parameter under study (temperature in this work). This can be analysed in terms of a simple three-level scheme, as it can be observed in the Figure 1.1

This method can use any pair of levels, however, certain energy levels follow a thermal dependence that conforms to Boltzmann's population distribution law, these being the thermally coupled levels (TCLs). Those that do not follow this temperature dependence are the non-thermally coupled levels (non-TCLs).

As it can be observed, the transitions between energy levels are ${}^2H_{11/2} \rightarrow {}^4 I_{15/2}$ and ${}^4S_{3/2} \rightarrow {}^4 I_{15/2}$. Due to the proximity of these energy levels, thermal excitation produces the regulation of population between the lower and upper levels [15].

Furthermore, the value of the ratio of the intensities does not vary with the laser source, since these emitted intensities are only determined by the proportional population of these levels. Despite this, it should be noted that a high power intensity of the laser source may heat the sample, affecting the *LIR* directly, thus low excitation powers shall be used. The relation of intensities allows us to characterize the emissions in correlation with the increment in temperature. As was mentioned above, the relative population of the two thermalized coupled levels (TCLs), can be described by a Boltzmann distribution following

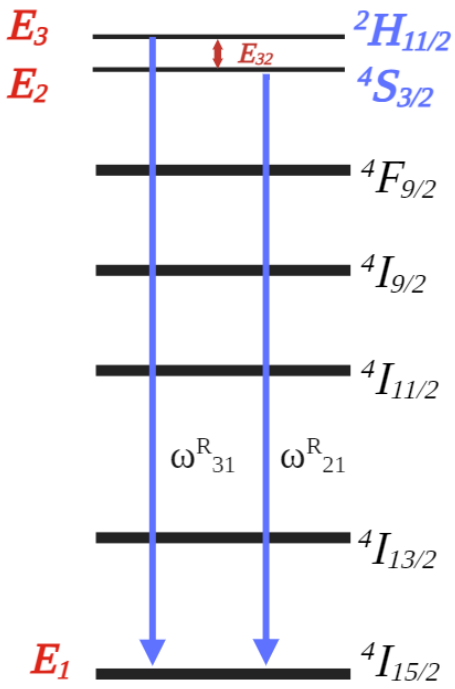

Figure 1.1. *Simplified representation of the three-level system of the Er^{3+} ion.*

the expression:

$$LIR = \frac{I_{31}}{I_{21}} = \frac{\omega_{31}^{R} g_3 h\nu_3}{\omega_{21}^{R} g_2 h\nu_2} e^{\frac{-E_{32}}{k_B T}} = Ce^{\frac{-E_{32}}{k_B T}} \tag{1.1}$$

The spontaneous emission rates ω_{31}^{R} and ω_{21}^{R} correspond to the transitions from the energies E_3 and E_2 to the E_1 level. The I_{ij} are the integrated intensities, g_i and g_j are the degeneracies *(2J+1)* of the levels, E_{ji} the energy gap between the i and j level, ν_i and ν_j the transition frequencies, k_B is the Boltzmann constant and T is the temperature. From now on in the text, the constants of this equation will be referred to as C.

The relative sensitivity S_{rel} is an important parameter in the characterization of a sensor, and it is widely used to compare its reliability regardless of its nature [16][17][18]. For an optical temperature sensor, it determines the relative change of the *LIR* in correlation with the upward trend of temperature and is expressed in units of $\%K^{-1}$ [19]:

$$S_{rel} = \frac{1}{LIR}\left|\frac{dLIR}{dT}\right| \cdot 100[\%] \tag{1.2}$$

In the case of thermalized coupled levels (TCLs) it can be obtained by deriving Eq. (1.1) with respect to temperature, as can be seen in Eq. (1.2) The resulting expression is:

$$S_{rel} = \left(-\frac{\Delta E_{32}}{k_B T^2} \right) \cdot 100[\%] \tag{1.3}$$

Whilst a greater energy gap between thermalized levels leads to a higher sensitivity, it also induces a lower intensity as a consequence of having a comparatively smaller population at the upper level.

In addition to the relative sensitivity S_{rel}, another parameter that determines the performance of the optical temperature sensor is the temperature resolution or uncertainty δT. It is defined as the smallest temperature increment that can be measured, and it can be obtained by a Taylor's series expansion of the temperature variation. Considering the contribution of the first term of the series expansion, the temperature resolution can be written as [20]:

$$\delta T = \frac{1}{S_{rel}} \frac{\delta LIR}{LIR} \tag{1.4}$$

where $\frac{\delta\ LIR}{LIR}$ is the relative uncertainty on *LIR*.

In this work, the temperature uncertainty will be estimated by two methods, by the application of the Eq.(1.4) and by performing 100 measurements of the spectra under the same conditions at 298, 323 and 373 K; which are temperatures that are representative of the range under study.

1.4.2 Upconversion

The phenomenon of upconversion (UC) is an interaction between light-matter in which photons are emitted at a high frequency due to an excitation of the sample by photons with low energy [21]. The most common lanthanide upconversion mechanisms are excited-state absorption (ESA) and energy-transfer upconversion (ETU).

ESA is a process in which a single excited ion absorbs an additional photon, and is promoted to a higher energy level, i.e. the successive absorption of two photons by the same ion occurs. As the temperature increases, the probability of non-radiative emissions also rises, thus leading to a decrease in emission intensity [22].

Energy-transfer upconversion (ETU) is the most efficient type of upconversion process, and it involves two groups of ions: the activator and the sensitizer. In this process, an ion (sensitizer) is excited to a higher energy level by the absorption of a photon, then transfer its energy to an activator ion that reaches a higher energy level. A possible second transfer from another sensitiser can excite the activator to a higher level, from which it decays radiatively [23].

The UC mechanism in our project involves a sensitizer, Yb^{3+}, and an activator, Er^{3+}, and the process is schematically illustrated in Figure 1.2

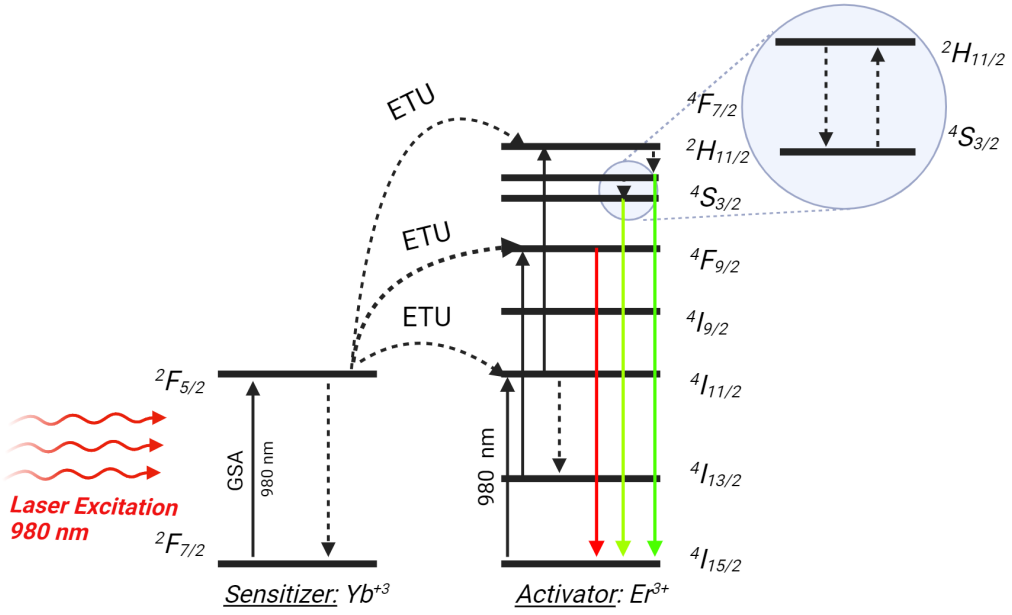

Figure 1.2. *Representation of the Upconversion Mechanism of Yb^{3+} and Er^{3+}, emphasizing on the TCLs of the Er^{3+} ions, $^2H_{11/2}$ and $^4S_{3/2}$ levels.*

In the ETU process among Yb^{3+} and Er^{3+} ions, a 980 nm laser was used as the excitation source. The Yb^{3+} ions absorb a photon to transit from the fundamental level $^2F_{7/2}$ to a higher level $^2F_{5/2}$. This transition is known as ground state absorption (GSA). Subsequently, the ETU takes place; transferring energy from the sensitizer (Yb^{3+}) to the activator (Er^{3+}). As a consequence, the Er^{3+} ions reach the excited energy level $^4I_{11/2}$ and, shortly thereafter, partly decaying to the level $^4I_{13/2}$. At this stage, this process continues, leading the population to the $^4F_{7/2}$ and $^4F_{9/2}$ levels due to the excitation of the electrons from the $^4I_{11/2}$ and $^4I_{13/2}$ levels, respectively. Consequently, the electrons that are on the $^2H_{11/2}$, $^4S_{3/2}$ and $^4F_{9/2}$ levels decay. Lastly, radiative transitions occur; which produces green and red emissions as a result of ground-level decay emitting photons. The emissions object of study are the energy transitions between $^2H_{11/2} \rightarrow ^4 I_{15/2}$ with emission at 525 nm and the emission at 550 nm corresponding to the transition $^4S_{3/2} \rightarrow ^4 I_{15/2}$.

Chapter 2

Methodology

Resumen

En este capítulo mostramos los tres procesos en los que hemos dividido la metodología, que incluye la caracterización de la muestra utilizada, la creación de una pieza 3D (tubo hueco), la aplicación de una mezcla homogénea de resina y un material ópticamente activo en el interior del tubo hueco y, finalmente, la realización de las medidas de temperatura en el tubo. En primer lugar, detallamos el montaje experimental y el procedimiento seguido para caracterizar el vidrio fluoroindato dopado con erbio e iterbio y poder analizar su viabilidad como sensor térmico óptico. Posteriormente, describimos los pasos que hemos llevado a cabo, tanto en el diseño, como en la impresión y la aplicación de la resina dopada en la pieza 3D, que en nuestro caso consiste en un tubo hueco. Finalmente, explicamos el montaje experimental y la realización de las medidas de la temperatura del flujo de agua por el tubo.

2.1 Materials

The sample used in this study was prepared with the following composition in *mol%*: $(40-\mathbf{x}-\mathbf{y})\cdot InF_3$, $20\cdot ZnF_2$, $20\cdot SrF_2$, $20\cdot BaF_2$, $\mathbf{x}\cdot YbF_3$ and $\mathbf{y}\cdot ErF_3$ where $\mathbf{x}=2.25$ and $\mathbf{y}=2.25$. The compounds used during the process were all 99.5% or a higher purity. The resulting mixture was heated for one hour at 673 K with $NH_4F\cdot HF$. Fluorides, produced by the conversion of residual oxide species, were formed by this process. Subsequently, the product was set to melt at 1175 K. The melt was then poured into an aluminium container previously heated to 523 K. Glass plates with thicknesses ranging between $1-2$ mm were produced.

2.2 Set Up (Printing and measuring equipment)

2.2.1 Calibration of the Luminescence Sensor

The first step in the methodology consisted in measuring the optical spectrum of emission on Yb^{3+} and Er^{3+} doped fluoroindate glass. This will allow us to determine the dependence of the luminescence ratio with temperature and the sensitivity of the ratio to small changes in temperature, in order to evaluate its performance as an optical sensor.

To study the material in powder form, first it had to be pressed to create a pellet. This pellet of material was placed between two microscope covers attached to a washer and placed inside a *Carbolite* horizontal tube furnace. A commercial 980 nm laser located at one of the furnace outlets was used during the calibration of the luminescence sensor. The laser excited the fluoroindate with a power of 450 mW while the furnace gradually raised the temperature. It must be taken into account that a high pump power of the laser can heat up the sample, altering the *LIR* measurements. To prevent this, a surface power density of 11.25 $\left[\frac{W}{cm^2}\right]$ was used, a power enough to give a good emission signal, but not enough to heat up the sample under study. The area of sample hit by the laser was evaluated, taking into account the *Full Width at Half Maximum (FWHM)* of the Gaussian profile.

To obtain the emission spectra, a 75 mm converging lens focuses the laser beam and excites the sample. Then, two lenses of 50.8 and 60 mm collect and focuses the sample emission in an optical fiber from *Ocean Optics* coupled to the *Avantes spectrometer*. Two optical filters: 800 nm long pass and 800 nm short pass, were used to avoid stray light when exciting the sample and acquiring the emission spectrum. Stray light is due to reflections from the laser or external light sources, such as the computer screen connected to the spectrometer. The elements of the set-up are numbered in Figure 2.1 and 75 and 60 mm lenses are not included in the picture.

Due to the operation of the furnace itself, the temperature at the sides of the furnace, where the sample is located, is not the same as that of the centre, being the temperature of the sample much lower than the one reached by the oven. Hence, a K-type thermocouple was placed to be in contact with the encapsulated sample while temperature readings were recorded. It should be taken into consideration that the thermocouple is in contact with the microscope covers in which the sample is encapsulated, not with the pellet itself. Nonetheless, a negligible variation of the temperature from the pellet to the covers is expected.

In order to obtain the evolution of the spectrum as a function of temperature, 50 emission spectra were obtained at different temperatures with an integration time of 10 ms, in the range from 296.8 K to 376.3 K.

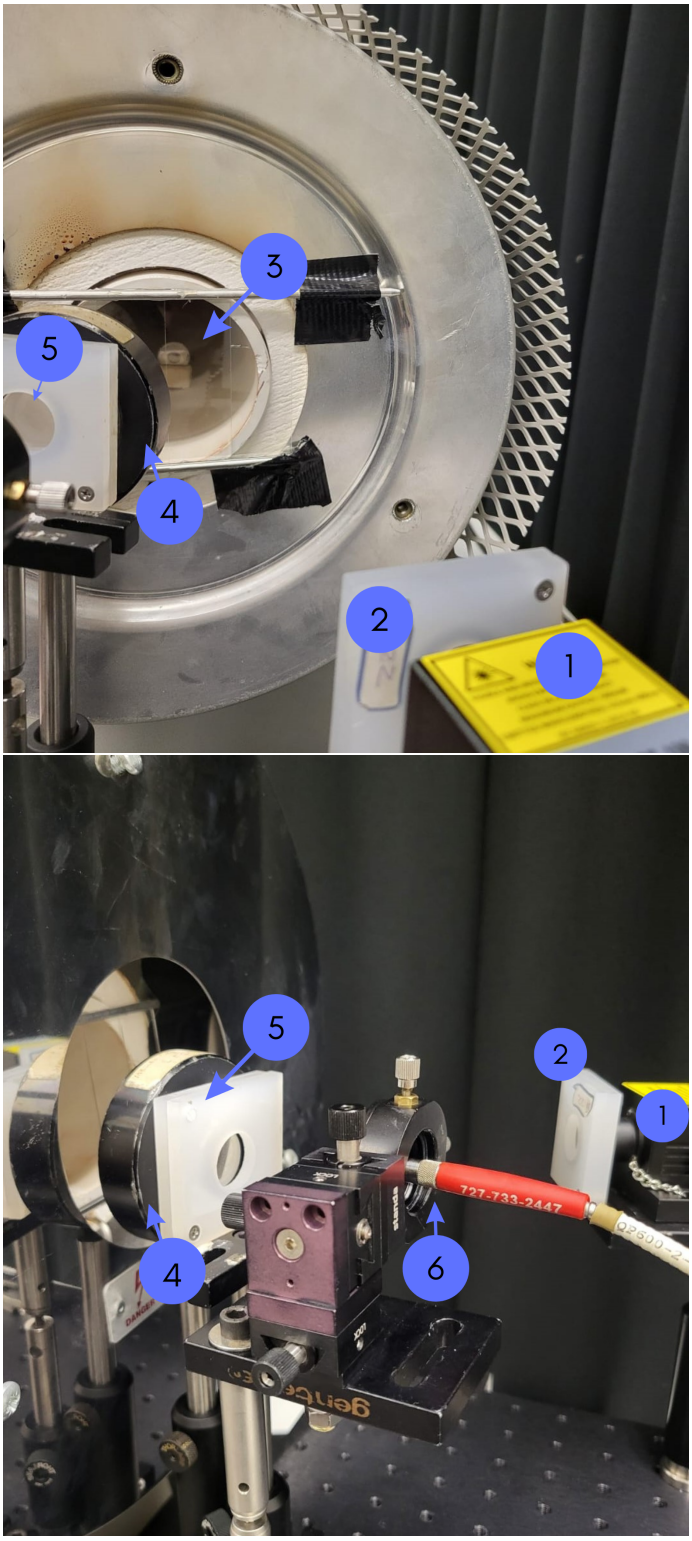

Figure 2.1. *Experimental setup for the luminescent sensor calibration. (1) 980 nm laser, (2) Long pass filter, (3) Sample, (4) 50.8 mm focal length lens, (5) Short pass filter (6) Optical fiber connected to the Avantes spectrometer.*

2.2.2 3D impression

This section will describe in detail the processes followed for the design and printing of the 3D piece used in this project.

A tubular piece was designed with a length of $l = 10\ cm$, an inner diameter of $\varnothing_i = 0.3\ cm$, an outer diameter of $\varnothing_o = 0.5\ cm$. The outer diameter was such that it could be easily connected to the thermal bath. Another tube with an inner diameter of $\varnothing_i = 0.4\ cm$ was also fabricated to see which model was more suitable for our project. On the other hand, the length of 10 cm was also chosen not only because it is a relatively standard measurement, but also due to the limitation of the 3D printer used. For the manufacturing of the tubes, a natural *3D870 SMARTFIL PLA filament* of 1.75 mm of diameter was used as raw material.

The prototypes were created with software Tinkercad, and the design was saved in surface tessellation language (STL). The STL file was then exported to Bambu Studio slicer in order to select the manufacturing parameters and generate the G-code file. Finally, from the G-code archive, the models were printed using a *Bambu Lab X1 Carbon* printer. During manufacturing, the chosen parameters were a layer width of 0.4 mm, a layer height of 0.2 mm, a 100 % infill pattern density, a bed temperature of 55 °C, an extruder temperature of 220 °C and a deposition speed of 40 mm/s.

Moreover, in the process of impression, a series of 6 tubes were printed to be able to decide on the most suitable piece due to possible deformations and thus minimize possible experimental errors. The printing process can be seen in Figure 2.2

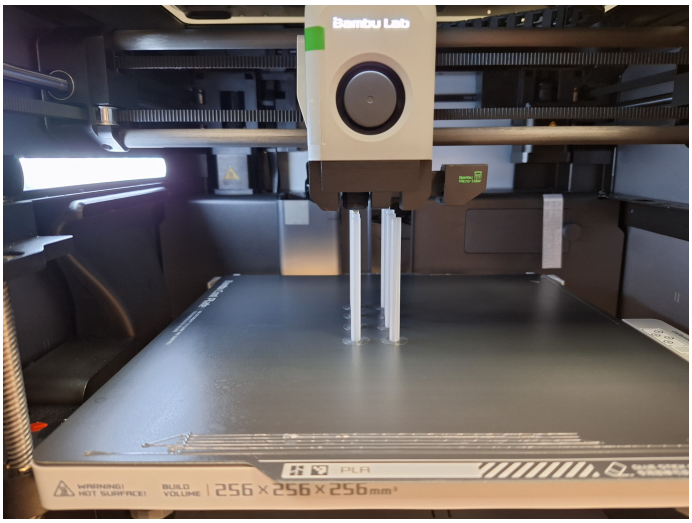

Figure 2.2. *A set of tubes made with PLA on the Bambu Lab X1 Carbon 3D printer. The inner diameters of the tubes were 3 and 4 mm, while the outer one was 5 mm.*

In order to be able to cover the inner walls of the tube with the luminescent material used in the project, a UV-curing resin was required. The resin employed was a *Professional UV Resin Blue Clear V2 Siraya Tech*, which consists in a mixture composition of urethane acrylate (CAS No. 877072-28-1, wt% =30–50%), acrylic monomer (CAS No. 64401-02-1, wt% = 30–50%), and photoinitiator (CAS No. 119-61-9, wt% = 0–5%). The resin was selected as a form to incorporate the luminescent material into the tube, since exposure to UV light causes the resin to solidify in a permanent and durable form.

For this purpose, the resin was mixed as homogeneously as possible with a certain amount of the powdered optical active material. A 95 % of the resin was mixed with a 5% of the fluorindate material. The resin-sample proportion was chosen to reach an appropriate equilibrium between having enough concentration of the optically active material to detect the emissions and not affecting the chemical composition of the resin itself. After 3D printing the part, the optically doped resin was embedded into the inner walls of the tube. This step was carried out using a pipette, impregnating the inside inner sides of the tube with the mixture and making sure that no area was left uncovered. Once the coating was finished, the curing process was carried out with a UV lamp. The resin transforms into a solid by exposure to UV rays. After an initial curing with the UV lamp, the piece was left in the laboratory in a controlled environment for a period of 2 days to ensure that complete drying was achieved.

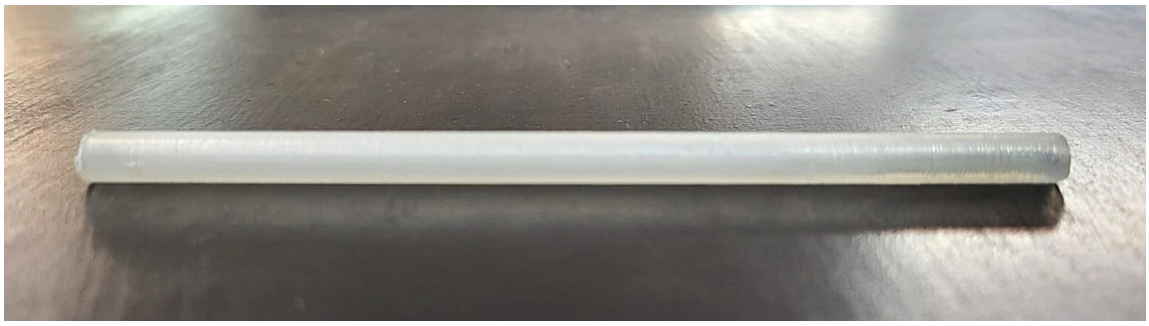

Figure 2.3. *Final 3D tube used in the study.*

Finally, due to the error of the 3D printer, the experimental dimensions obtained were $l = 10.08\ cm$ (length), $\varnothing_i = 0.21\ cm$ (inner diameter) and $\varnothing_O = 0.48\ cm$ (outer diameter). The final piece can be seen in the Figure 2.3

2.2.3 Thermal bath

The third and final part of the methodology is the implementation of the optical sensor as the doped tube, from now on DT. Through the doped tube, a liquid will flow and its temperature will be measured.

The optically active material is excited by a 980 nm laser. Measurements of the emitted spectrum will be obtained, at the centre and at both ends of the tube. The chosen liquid for this study was water due to its well documented thermal properties, high heat capacity, non-toxic and for its possible compatibility with industrial and biological applications. It should be highlighted that the emission spectrum comes from the inner walls of the tube closest to the laser, which is the area that is doped. Therefore, the level of spectral transparency of the fluid should not be taken into account, as this will not affect our measurements.

In order to heat the water, the DT was connected to a thermal bath. This thermal bath was equipped with a pumping machine that enabled the water to flow through the tube. A thermostat placed in the tank allowed the control of the temperature of the water at any given time and a bifurcation was created to reduce the velocity of the flow. By decreasing the water velocity, a more accurate measurement of the temperature in the DT is possible. This modification of the set-up was crucial to significantly improve our measurements and thus our results. In addition, to control the flow of water through the tubular piece, two flow control valves were placed at the entrance of the tube.

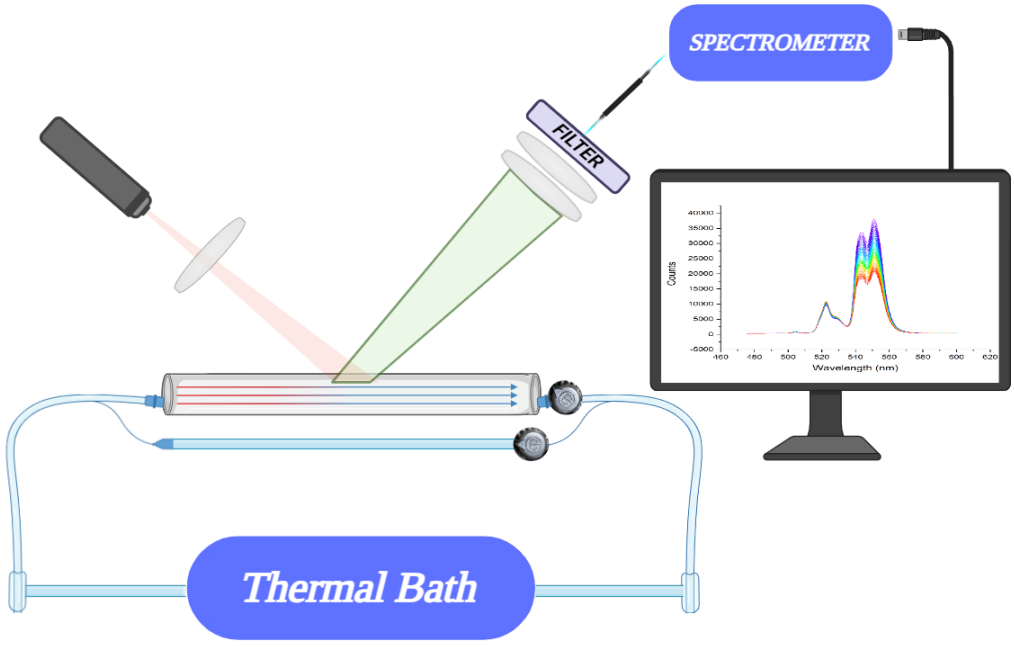

Figure 2.4. *Experimental set-up used for the detection of the temperature of the fluid flowing through the tube.*

To study the emissions in all the tube length, the tube was placed on an optical rail, allowing the tube movement while keeping the laser and the detection set-up fixed. A 980 commercial laser, with a power of 450 mW, was focused with a 75 mm converging lens and used to excite the doped tube. Two converging lenses of 50.8 and 60 mm focal length were used to collect and focus the emitted light in an optical fiber which was connected to a spectrometer ($Andor\ Newton^{EM}$). An 800 nm short pass filter was used in order to avoid stray light. The experimental set-up used is represented in the Figure 2.4

A series of measurements were carried out in this set-up, with two objectives. The primary objective was to be able to measure the temperature of a running-through liquid with an effective, safe and non-invasive procedure. The second objective was to determine the temperature difference from the beginning to the end of the tube.

In addition, the mass flow rate was calculated. This yielded a value of 0.04 grams per second. For this measurement, the end of the tube was disconnected from the thermal bath while the pump was operating and the water collected for 20 minutes. Finally, the water was weighted and the resulting mass was obtained.

$$Q_m = \frac{42.46\ [gr]}{1200\ [s]} = 0.04\ [gr/s] \tag{2.1}$$

Chapter 3

Results and Discussion

Resumen

En este capítulo se presentan los resultados obtenidos mediante la metodología anteriormente explicada. En primer lugar, exponemos los parámetros clave obtenidos ajustando los valores del *LIR* a una distribución de Boltzmann: el valor del *Energy Gap*, la sensibilidad relativa y la incertidumbre de la temperatura. Se obtuvo una sensibilidad máxima relativa de 1.16 ($\%K^{-1}$) a 296.8 K, con una incertidumbre de temperatura mínima de 0.5 K.

Por otra parte, se detallan los resultados obtenidos en el estudio de la temperatura del agua que fluye a través del tubo y se discuten la calidad de los mismos. Este estudio de la temperatura del tubo se ha realizado mediante tres análisis: el primero tiene como objetivo la medición de los espectros de emisión al principio del tubo con el aumento de la temperatura del baño térmico, el segundo tiene el objetivo de obtener la diferencia de temperatura entre el principio y final del tubo y el último el estudio de las desviaciones estándares a distintas temperaturas. Por último, para determinar su precisión, se ha realizado un estudio de repetibilidad de las medidas, obteniendo una repetibilidad máxima de 99,92 %.

3.1 Results of the luminescence optical material

In order to characterize the fluorindate glass doped with Yb^{3+} and Er^{3+}, the emission spectra were taken at different temperatures, as can be seen in Figure 3.1

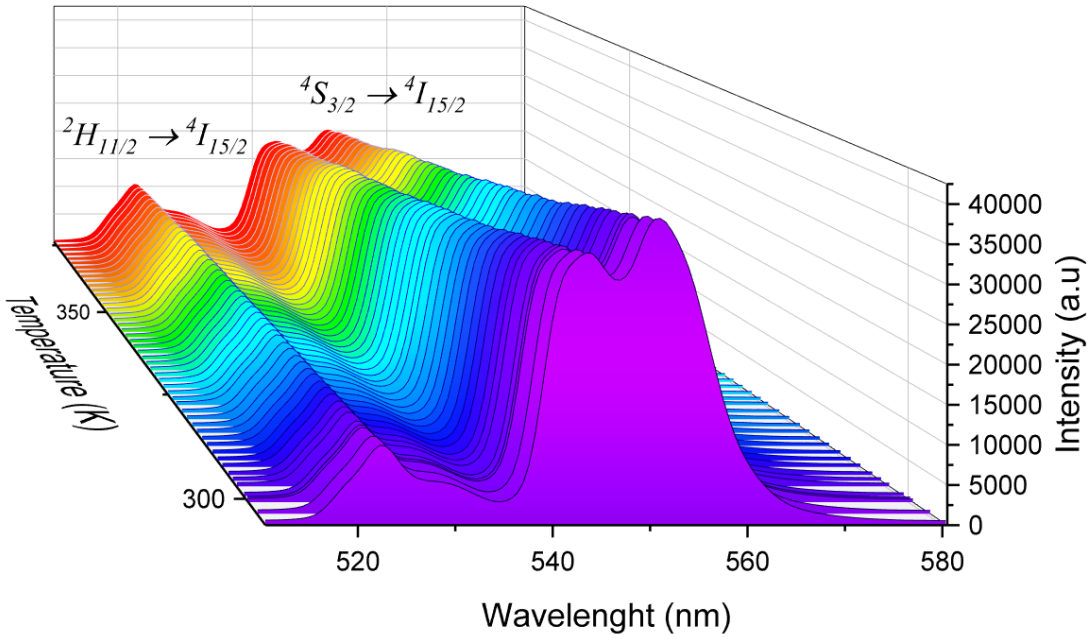

Figure 3.1. *Emission spectra from 510 to 580 nm as function of the temperature for the upconversion emissions of the fluoroindate glass under 980 nm excitation.*

Two intense emissions can be observed at wavelengths around 525 nm and 550 nm. As was mentioned in the second chapter, these emissions correspond to the transitions $^2H_{11/2} \rightarrow^4 I_{15/2}$ and $^4S_{3/2} \rightarrow^4 I_{15/2}$ for the 525 nm and 550 nm intensity peaks, respectively.

The evolution of the spectrum as a function of temperature was measured, showing the strong temperature dependence of the ratio of intensities of the 525 nm and 550 nm bands. The emission corresponding to the 550 nm transition decreases with increasing temperature. This behaviour is a direct consequence of thermally induced population migration from lower ($^4S_{3/2}$) to higher ($^2H_{11/2}$) levels.

Applying the *LIR* technique, a relation between temperature and intensity can be acquired, which allows the sample to work as a thermal optical sensor. The results are presented in Figure 3.2

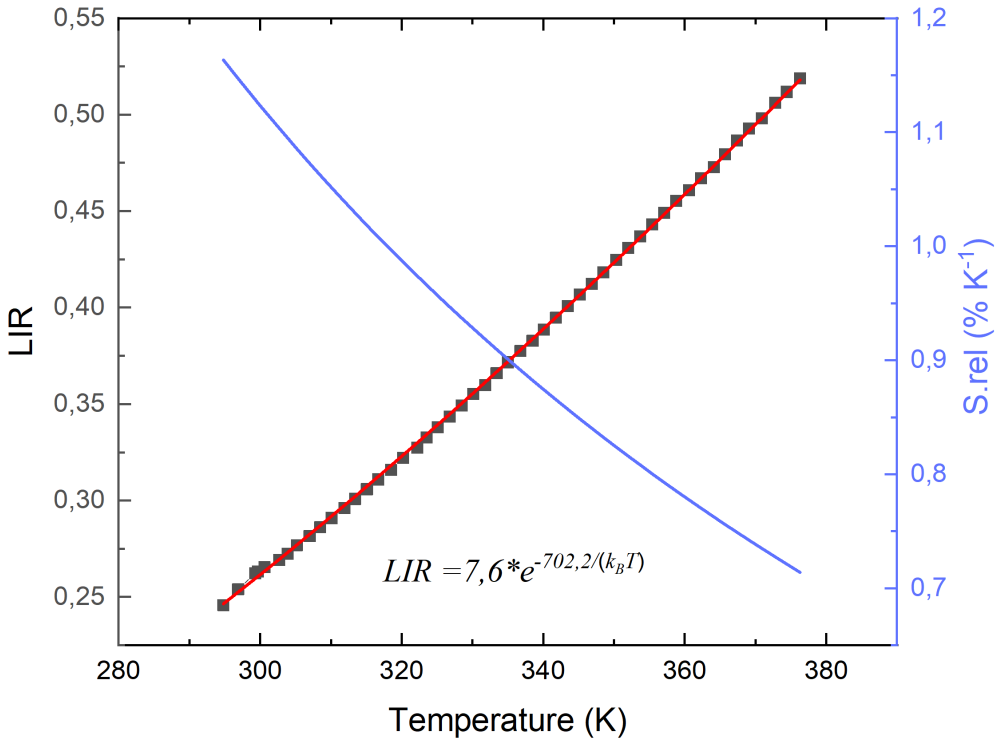

Figure 3.2. *Experimental values of LIR as a function of temperature (■) fitted to the Boltzmann distribution law, Eq. 1.1 (▬). Also is included the sensor relative sensitivity S_{rel} represented as (▬).*

The LIR data were fitted to a Boltzmann distribution, given by Eq. 1.1, obtaining an Energy gap of $E_{32} \approx 702.2\ cm^{-1}$, a constant $C = 7.61$ and an $R^2 = 0.999$. The *LIR* values range from 0.25 to 0.52 for a temperature increment of 81.5 K. On the other hand, the values of the relative sensitivity S_{rel} vary from 0.7 to 1.2 $(\%K^{-1})$ on the temperature range under study (from 296.8 to 376.3 K).

The maximum value of the relative sensitivity achieved with the fluoroindate glass was 1.16 $(\%K^{-1})$ at 296.8 K. These results were compared with other $Er^{3+} - Yb^{3+}$-doped compositions and presented in Table I. In the same temperature range, our sample has a similar sensitivity than $GdV0_4 : Er^{3+}/Yb^{3+}$ and a similar temperature uncertainty. The other results shown in the Table I have different temperature range and are not suitable for comparison.

The relative sensitivity gradually decreases as the temperature increases for most of the Er^{3+}-Yb^{3+}-doped materials. This enables us to utilize the fluoroindate in a temperature range close to room temperature and obtain results with an high sensitivity. Hence, we can conclude that this material is suitable to cover the inner walls of the tube and determine the temperature of the flowing water, measuring in this case in a temperature range of 294 to 323 K.

Table I: *Maximum relative sensitivity and other relevant parameters for comparison of multiple Er^{3+}/Yb^{3+} based temperature optical sensors.*

Sample	Range of Temperatures (K)	$S_{rel}(\%K^{-1})$	Minimum uncertainty	Ref
Fluorindate glass: Er^{3+}/Yb^{3+}	295 – 376	1.16	0.5	This work
$YAP : Er^{3+}/Yb^{3+}$	296 – 600	1.23	0.4	[15]
$BiPO_4 : Er^{3+}/Yb^{3+}$	313 – 573	1.03		[24]
$LaBMoO_6 : Er^{3+}/Yb^{3+}$	298 – 578	1.16		[25]
$\beta - BiNbO_4 : Er^{3+}/Yb^{3+}$	150 – 500	3.70		[26]
$NaLaMgWO_6 : Er^{3+}/Yb^{3+}$	293 – 553	1.07		[27]
$GdVO_4 : Er^{3+}/Yb^{3+}$	297 – 370	1.17	0.4	[28]

In order to estimate the temperature uncertainty, 100 measurements were taken in the same condition and at three different temperatures, with an integration time of 10 ms. The temperatures were calculated from the *LIR* values by using the calibration shown in Fig. 3.2 The histograms taken for each temperature with their respective standard deviations are shown in Figure 3.3 As it can be appreciated, the histograms follow a Gaussian distribution, centred in the expected value of temperature. The standard deviations obtained for the three temperatures were 0.5, 0.6 and 0.9 K, respectively.

The temperatures chosen for the study were 298 K, which corresponds to the typical room temperature, 323 K, which is the highest temperature for the study of the water-flowing 3D tube, and 373 K, temperature close to the maximum temperature used in the sample calibration. This temperature, 373 K, is not only our maximum temperature but also the temperature with a higher uncertainty. This is because, as shown in Figure 3.2 the higher the temperature of our sample, the lower the relative sensitivity and, consequently, the higher the temperature uncertainty will be.

In addition, the uncertainty of the temperature was obtained theoretically by applying Eq. (1.4), where δLIR is the uncertainty of the *LIR*. The value of the *LIR* uncertainty was estimated using the standard deviations of each *LIR*. The results are shown in Figure 3.4 Both methods obtained similar temperature uncertainty (δT), showing the same upward character with increasing temperature. This is a consequence of the inversely proportional dependence of the temperature uncertainty expression on the relative sensitivity.

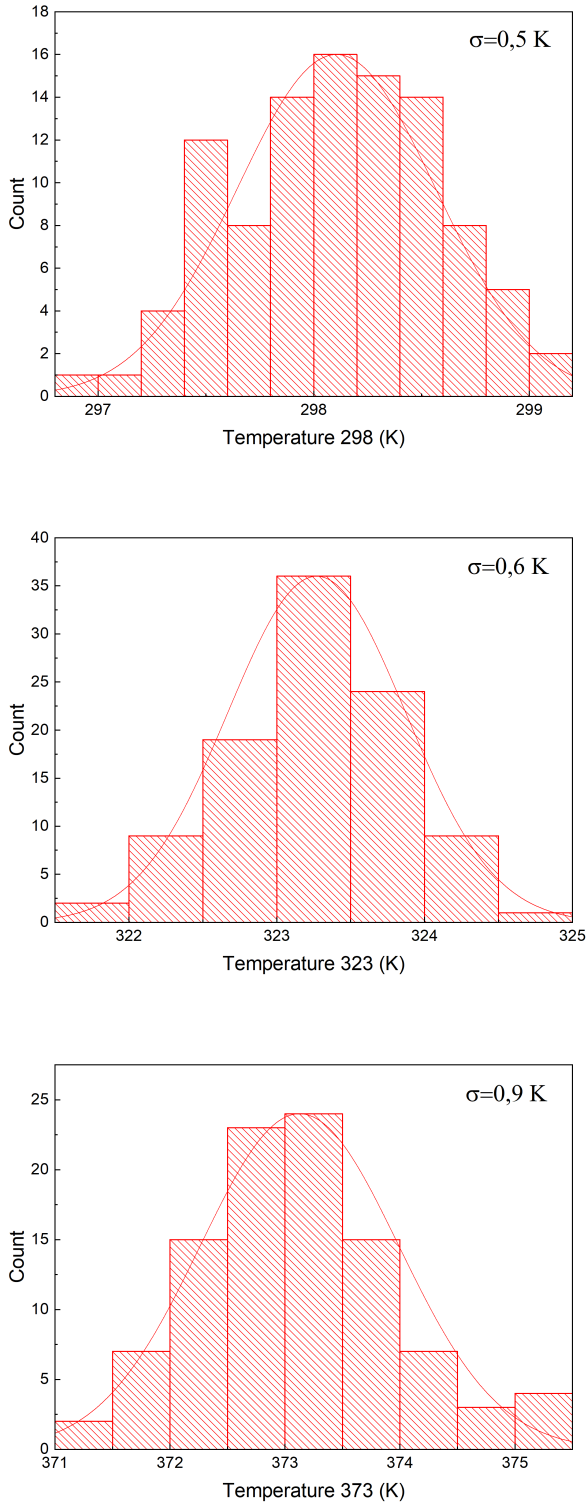

Figure 3.3. *Histograms of the 100 experimental measurements acquired at 298, 323 and 373 K with their respective standard deviations.*

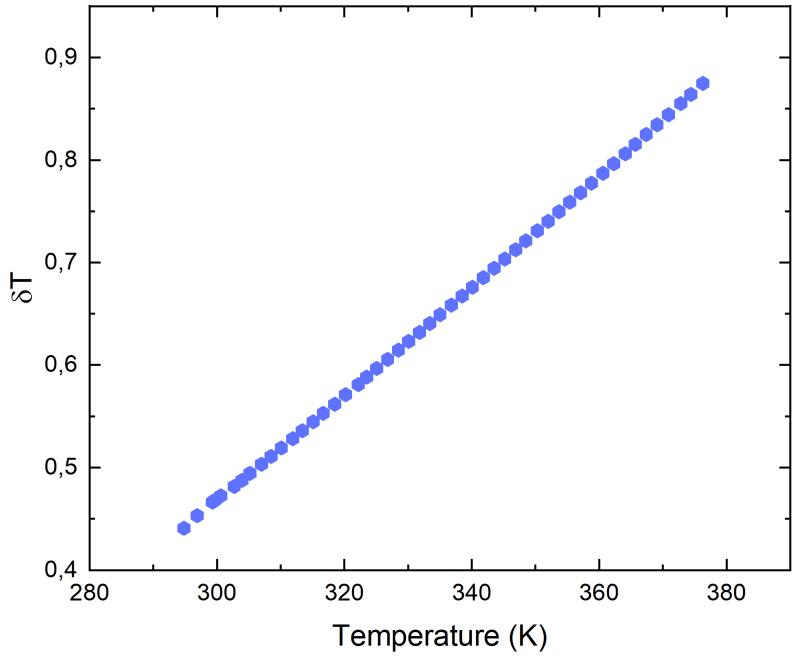

Figure 3.4. *Theoretical estimation of the temperature uncertainty δT (⬢).*

3.2 Results of the 3D printed tube as a thermal optical sensor

3.2.1 Temperature of the tube

In order to measure the temperature in the tube, it must be taken into account that the temperature applied in the thermal bath is not the same as that of the water which reaches our doped 3D part. As a consequence of the thermal conductivity of the bath tubes, heat dissipation occurs throughout the water path. Three types of measurements were carried out: in the first one, the emission spectra in the beginning of the tube was measured for increasing values of the temperature of the thermal bath. These emission spectra were obtained in several values of the temperature, from 296 to 323 K. In the second set of measurement, temperatures values were measured at the beginning and at the end of the tube, alternating in each measurement. With this data, the temperatures measured at the beginning and at the end of the tube were compared with those obtained with an external sensor. These measurements will also be used for a repeatability study. Finally, a series of measurements were taken in the centre of the tube in order to obtain the standard deviations at 294, 310 and 323 K.

The values of the estimated temperature obtained from the spectra measured at the beginning of the tube were represented in function of the temperature of the thermal bath and can be seen in Figure 3.5

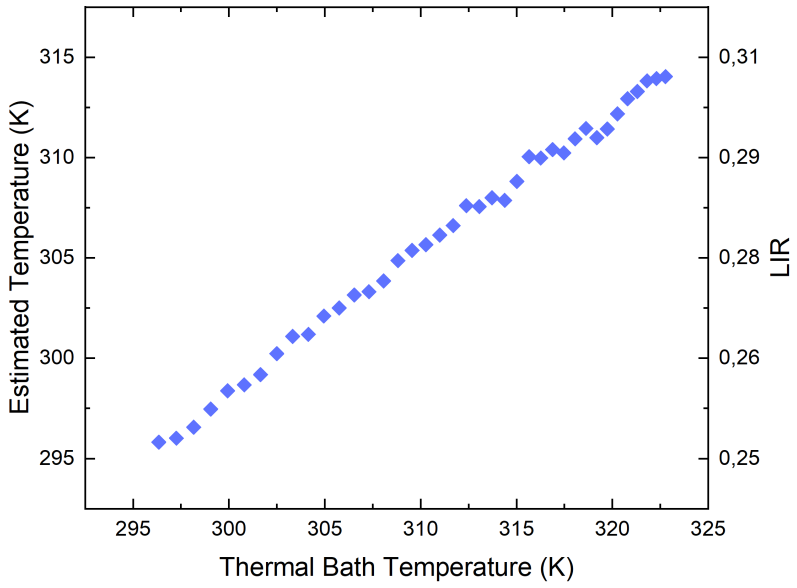

Figure 3.5. *Experimental temperatures and LIR (♦) obtained by the spectra in the beginning of the tube with the corresponding thermal bath temperature.*

As can be observed, the dependence between the temperature of the thermal bath and the estimated temperature in the DT is linear. Furthermore, the fit of these values has a positive slope of less than one, which implies that there is a significant temperature drop between the temperature given by the thermostat and the one reaching the tube, as a consequence of the path of the water through the set-up.

In addition, as explained before, a series of 10 measurements were made at the end and the beginning of the tube with a thermal bath temperature of 323 K, to obtain the difference of temperature. The results obtained in our measurements are shown in Figure 3.6 The mean temperature values obtained at the inlet and outlet of the water are 314.59 and 307.49 K. Hence, the average temperature difference obtained along the tube is:

$$\nabla T = \frac{T_{beg.} - T_{end}}{l_{tube}} = \frac{314.59 - 307.49}{10.08} = 0.70 \left[\frac{K}{cm}\right] \tag{3.1}$$

This average temperature difference quantifies the thermal efficiency of the system and provides information on how much the temperature varies per cm.

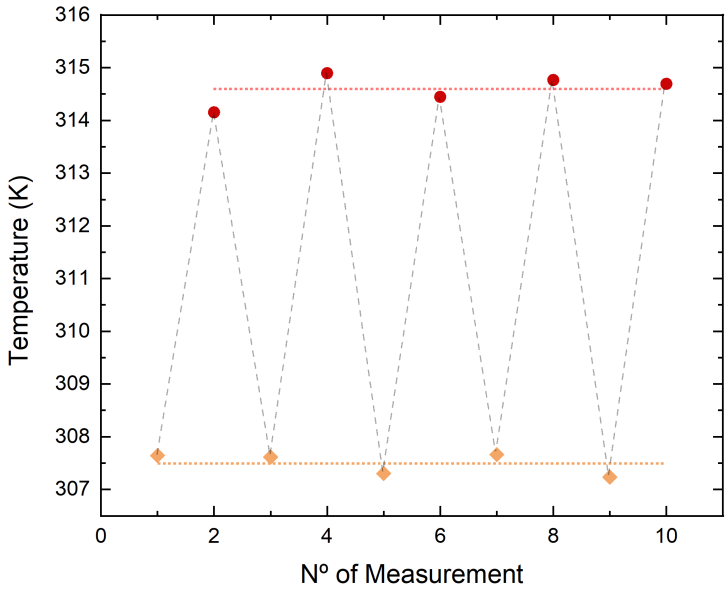

Figure 3.6. *Experimental values recorded alternating between the beginning* ● *and the end of the tube* ♦*, showing the repeatability of the measurements.*

The temperature values obtained do not significantly differ, with a maximum difference between them of 0.7 K for the water inlet and 0.4 K for the outlet. These fluctuations may be caused by the experimental set-up itself, which was not protected from external perturbations such as air currents and so is susceptible to small temperature changes. Furthermore, these variations are coherent if we take into account the temperature uncertainty obtained for the calibration of the sample being in the range 0.5-0.6 K approximately for temperatures between 298 and 323 K, Figure 3.3. In addition, if a comparison is made between the results of the Figure 3.5 taken in the beginning of the tube and the ones discussed, it can be observed that both temperatures at the beginning of the tube are very similar, differing by only 0.2 K. This deviation may be due to several experimental reasons. The measurements made at the beginning (Figure 3.5) for different temperatures and those made at both ends of the tube (Figure 3.6) were taken on different days, where the experimental conditions such as humidity, room temperature or room pressure were not the same.

Also, temperature measurements were made at the outlet and inlet of the water flow in the DT with a platinum sensor to compare with the temperatures obtained experimentally. The platinum sensors measure in the temperature range between 73 and 1273 K and they are precise and work reliably under a wide range of environmental conditions [29]. The temperatures measured at the inlet and outlet of the tube were 314.75 and 308.35 K, respectively. Comparing the average temperature obtained from our measurements with the platinum sensor measurements, it can be determined that there is a difference of 0.2 and 0.9 K. It can be seen that they do not differ by more than 1 K. Therefore, not only the error due to our measuring system, but also the error due to the accuracy of the platinum sensor,

which is determined by its sensitivity, must be taken into account.

For clarity, we present a table with the temperatures corresponding to the different measurements, according to each sensor and tube position, Table II.

Table II: *Temperatures of the Thermal Bath, Estimated Temperature and Temperature measured by the Platinum sensor (K) for each measurement position in the doped tube.*

Position in the DT	T. of the Thermal Bath (K)	Estimated Temperature (K)	T. Platinum Sensor (K)
Beginning	323.0	314.6	314.8
End	323.0	307.5	308.4

For the study of uncertainties, 100 measurements were made at different temperatures. From Figure 3.5 can be seen that the corresponding estimated temperatures for the 294, 310 and 323 K are 289.8, 305.3 and 314.4 K for the temperature at the thermal bath.As it can be appreciated in the Figure 3.7, the data are approximately centred on the values that were expected of temperature. The three mean temperatures obtained for these histograms are 289.8, 304.8 and 314.2 K.

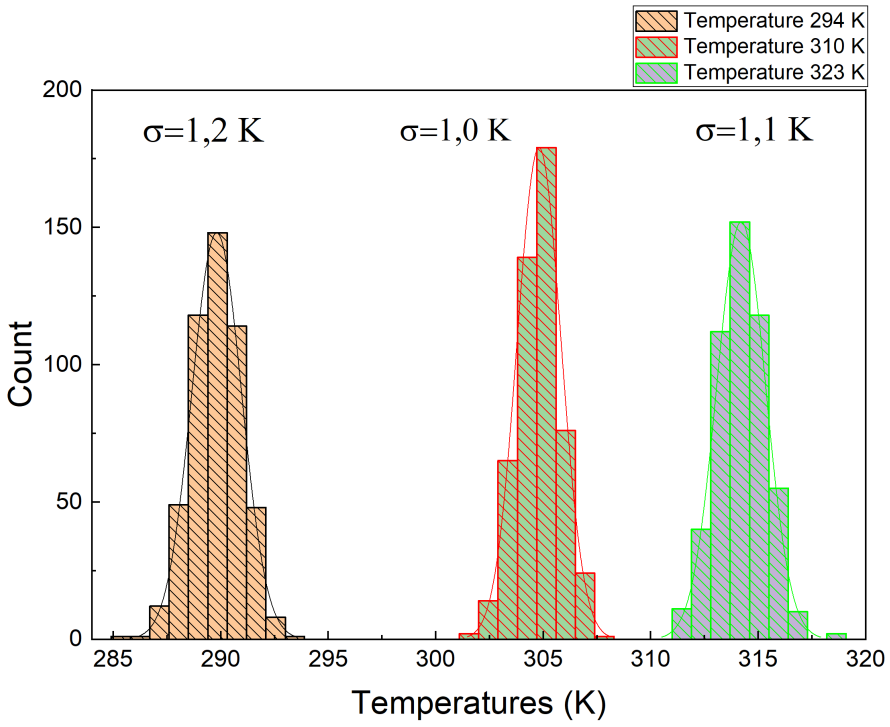

Figure 3.7. *Histogram of the corresponding Estimated Temperatures at 294, 310 and 323 K in the Thermal Bath, with the respective standard deviations.*

Moreover, the distributions of the histograms follow a Gaussian distribution. The standard deviation for the three temperatures were 1.2, 1.0 and 1.1 K, respectively. This high values of standard deviation are an indication that these methods makes it difficult to measure small temperature differences and therefore limits our analysis. Furthermore, the temperature uncertainty in this case does not follow the expected trend in correlation with sensitivity. That is, as can be seen in the standard deviations of the histograms, Figure 3.3, the higher the temperature, the higher the uncertainty. The cause of this behaviour is due to possible changes in environmental conditions. A small displacement of the tube in relation to the optical system or vibrations caused during the measurements can be a direct source of this error. In addition, the reliability of the thermostat of the thermal bath is crucial, and its possible instability when heating the tank could lead to further deviations in the temperature data.

3.2.2 Repeatability

Repeatability is one of the key factors in the successful application of data analysis methods in the measurement of errors. Consistent and replicable results are a crucial factor in the terms of scientific work.

This concept was first introduced in 1986 [30] and has been widely adopted throughout the scientific community, and it permits to evaluate the reliability of measurements conducted by a particular method. Many research papers have given different approaches to this terminology, resulting in various conceptions of repeatability for each scientific work or area of study [31]. Thus, the definition of repeatability used in this work refers to the degree of concordance or agreement between the outcomes of successive measurements of the same experiment conducted under identical conditions [32].

To characterize the repeatability of the results obtained, a cycle of measurements was performed, alternating from measurement to measurement, taking the spectrum at the beginning and the end of the tube. For this matter 10 measurements were taken along the tube, Figure 3.6 The repeatabilities of the temperatures obtained were calculated by the expression:

$$R = \left(1 - \frac{\max(|\ \Delta_c - \Delta_i\ |)}{\Delta_c}\right) \cdot 100\% \tag{3.2}$$

Where Δ_c is the mean value obtained and Δ_i are each values for the temperatures. A repeatability of 99,86 % for 314 K and 99,92 % for 307 K was archived for the data of the Figure 3.6 This high repeatability suggests that reliable results may be attainable.

Chapter 4

Conclusion

Resumen

En este capítulo se exponen las conclusiones fundamentadas en los resultados obtenidos a lo largo de este trabajo. Se consiguió en este proyecto desarrollar exitosamente un sensor óptico térmico con una estructura de tubo hueco. Mediante la técnica del LIR se obtuvo la relación de la dependencia térmica del espectro de emisión de la muestra bajo estudio, logrando obtener una sensibilidad relativa máxima de 1.16 $\%K^{-1}$ a 296.8 K y una resolución de temperatura de 0.5 K. Además, destacamos el éxito en el diseño y fabricación de la pieza 3D así como el dopaje de la misma. Finalmente, se realizó el análisis de la temperatura del líquido fluyendo a través del tubo. Pese a las limitaciones dadas por la incertidumbre de la temperatura de la muestra, se pudo medir la temperatura en los extremos del tubo, obteniendo un gradiente de temperatura de 0.70 K/cm. Se concluye, por tanto, que se ha conseguido cumplir los objetivos propuestos en este estudio teniendo en cuenta las limitaciones con las que nos hemos encontrado.

The principal aim of this project was to obtain a functional optical sensor by doping a tube created using 3D printing technology. Focusing on the results obtained, each objective proposed in this project could be met satisfactorily with the desired outcome, thus successfully developing an optical thermal sensor in a hollow tube format.

The relationship between the increase in temperature and the corresponding emission spectra could be obtained using the *LIR technique*. This enabled us to relate the *LIR* value to the different temperatures successfully. The results of this research show the feasibility of this sample to be used as a high-performance optical temperature sensor. A maximum relative sensitivity of 1.16 ($\%K^{-1}$) was achieved at 296.8 K, with a minimum temperature uncertainty of 0.5 K. The highest relative sensitivity range is found at temperatures from 296.8 to 323 K, making it ideal for our study with water.

It is worth explaining that the major focus point of this work was in the study of the temperature gradient along the tube, thus being able to analyse the decrease of the temperature gradient. Overall, the problem with this approach is that due to the minimum temperature uncertainty obtained in the characterization of the sample being 0.5K, significant temperature changes could not be detected in analysis where small sections of the tube are measured.

A hollow tube has been designed and created using 3D technology, which by applying a mixture of resin and the sample could be used as an optical thermal sensor. Thanks to this, it has been possible to estimate the temperature of the liquid flowing through the tube. In addition, the average gradient of temperature has been obtained, which value was 0.70 $\left[\frac{K}{cm}\right]$. However, this gradient could only be obtained by analysing the temperature at two points, at the beginning and at the end of the tube. These results suggest that the thermal coefficient or the relative sensitivity are not enough to appreciate large temperature changes between small sections of the tube. It is worth noting that this method of measurement, being non-invasive, allows us to measure the temperature of the flowing liquid without causing any disturbance to the liquid. This is a significant advantage over conventional sensors and has enabled us to obtain reliable results.

One important matter to discuss is that the standard deviations obtained for the measurement of tube temperatures are between 1.0 and 1.2 K. It must be taken into account that these values are higher than those obtained with the luminescent sample in the furnace. Such an increment could be explained in terms of possible changes in environmental conditions. For example, the temperature control in the thermal bath.

For all the above reasons, we can therefore conclude that the tube created by 3D printing is functional as an optical thermal sensor and has a wide range of promising applications in industry.

4.1 Future work

Due to the possible applications to industry, we will propose future works to determine the optimal direction of the extension of this study. Further experimental studies should aim to focus on not only exploring new designs where to implement the ideas presented but also study the possible industrial applications.

Further studies could be carried out on the resistance of these tubes to the abrasion of highly saline or abrasive solutions to see if it would be feasible to use them with other types of liquids. It should be noted that the material used in the printing, the biodegradable plastic PLA; and the resin used to dope the tube, *Siraya Tech Resin*; do not specify the resistance to chemicals, therefore certain possible applications of the tube cannot be discussed without further study.

A study of the upconversion emission spectra may be done at different powers to obtain the correlation of the intensity ratios as a function of pump power. This study should take into account which is the maximum pump power to avoid heating effect in the sample. This could improve the understanding of the sample in order to determine in which power pump it has the best performance and to generalize the study with different physical parameters.

In addition, a study of the spectra should be carried out in order to also characterise the variation of the spectra according to changes in pressure. This allows us to broaden the possible industrial applications of our project. By means of the *LIR technique* and the use of the doped tube (DT), the pressure to which a fluid is subjected inside the tube could be measured non-invasively and effectively. This potential feature would be particularly interesting for the waterjet cutting technique, by which hard materials such as marble can be cut using water with high pressure. Waterjet cutting is an innovative technique used broadly in the industrial field due to its high precision and versatility. By applying the LIR-based pressure measurements, it is likely to continuously detect the pressure of the water jet based on real-time data. This could potentially enhance the efficiency and safety of waterjet cutting procedures.

Another possible improvement proposed it might be to refine the process of mixing the sample with the resin. The mixing was done manually, trying to make it as homogeneous as possible, however, by using an ultrasound machine this process would be more efficient, and it would obtain much better results.

In addition, other promising designs can also be envisaged. Two designs that could be adapted to this method would be a ring and a spiral-shaped tube.

The ring design would be an adaptation of our design but with a much shorter length. The main idea behind this design would be to create a part that could be adapted and attached to large industrial tubes. This would permit this technology to be efficiently adapted to the industry, allowing the creation of optical thermal sensors at strategic points along the

industrial installation in order to obtain temperature and pressure measurements at those points.

Another design we could consider would be the tube with a spiral shape, as illustrated in Figure 4.1 The main advantage behind this design is that at a moderate tube length, the liquid would have much more travel compared to a straight tube. This would allow the liquid, being in contact with the surface and cooling down for a longer time, thus facilitating the measurement of the temperature gradient after each loop. Furthermore, the temperature difference per loop and therefore per area could be obtained, with interesting practical applications.

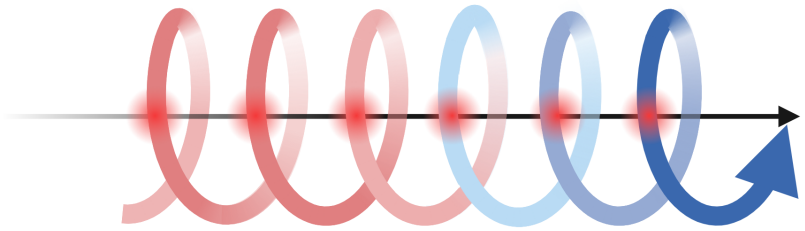

Figure 4.1. *Visual representation of the concept tube design. The remarked points would be the proposed points to be excited by the laser.*

Finally, a study with different types of liquids could be carried out. Furthermore, an interesting possibility with wide applications would be the use of the doped tube (DT) for a flow of gases at a certain temperature instead of liquids. However, it has to be taken into account that its handling and study can be more complex.

References

[1] Luca Ferrari, Luigi Rovati, Paola Fabbri, and Francesco Pilati. Disposable fluorescence optical ph sensor for near neutral solutions. *Sensors*, 13(1):484–499, 2013. ISSN 1424-8220. doi: 10.3390/s130100484. URL https://www.mdpi.com/1424-8220/13/1/484.

[2] Xu-dong Wang, Otto S. Wolfbeis, and Robert J. Meier. Luminescent probes and sensors for temperature. *Chem. Soc. Rev.*, 42:7834–7869, 2013. doi: 10.1039/C3CS60102A. URL http://dx.doi.org/10.1039/C3CS60102A.

[3] Daniel Jaque and Fiorenzo Vetrone. Luminescence nanothermometry. *Nanoscale*, 4: 4301–4326, 2012. doi: 10.1039/C2NR30764B. URL http://dx.doi.org/10.1039/C2NR30764B.

[4] Antonio Benayas, Eva Hemmer, Guosong Hong, and Daniel Jaque. *Near Infrared-Emitting Nanoparticles for Biomedical Applications*. Springer, 01 2020. ISBN 978-3-030-32035-5. doi: 10.1007/978-3-030-32036-2.

[5] Carlos D. S. Brites, Patricia P. Lima, Nuno J. O. Silva, Angel Millán, Vitor S. Amaral, Fernando Palacio, and Luís D. Carlos. A luminescent molecular thermometer for long-term absolute temperature measurements at the nanoscale. *Advanced Materials*, 22(40): 4499–4504, 2010. doi: https://doi.org/10.1002/adma.201001780. URL https://onlinelibrary.wiley.com/doi/abs/10.1002/adma.201001780.

[6] Jean-Claude G. Bünzli. Lanthanide luminescence for biomedical analyses and imaging. *Chemical Reviews*, 110(5):2729–2755, 2010. doi: 10.1021/cr900362e. URL https://doi.org/10.1021/cr900362e. PMID: 20151630.

[7] Kevin M McCabe and Mark Hernandez. Molecular thermometry. *Pediatric research*, 67(5):469–475, 2010.

[8] Guanying Chen, Hailong Qiu, Paras N. Prasad, and Xiaoyuan Chen. Upconversion nanoparticles: Design, nanochemistry, and applications in theranostics. *Chemical Reviews*, 114(10):5161–5214, 2014. doi: 10.1021/cr400425h. URL https://doi.org/10.1021/cr400425h. PMID: 24605868.

[9] Syed Fouzan Iftekar, Abdul Aabid, Adibah Amir, and Muneer Baig. Advancements and limitations in 3d printing materials and technologies: A critical review. *Polymers*, 15(11), 2023. ISSN 2073-4360. doi: 10.3390/polym15112519. URL https://www.mdpi.com/2073-4360/15/11/2519.

[10] Choon Wee Joel Lim, Kim Quy Le, Qingyang Lu, and Chee How Wong. An overview of 3-d printing in manufacturing, aerospace, and automotive industries. *IEEE Potentials*, 35(4):18–22, 2016. doi: 10.1109/MPOT.2016.2540098.

[11] Christian Iffelsberger, Daniel Rojas, and Martin Pumera. Photo-responsive doped 3d-printed copper electrodes for water splitting: Refractory one-pot doping dramatically enhances the performance. *The Journal of Physical Chemistry C*, 126(21):9016–9026, 2022. doi: 10.1021/acs.jpcc.1c10686. URL https://doi.org/10.1021/acs.jpcc.1c10686.

[12] L. Catarinucci, F. P. Chietera, and R. Colella. Permittivity-customizable ceramic-doped silicone substrates shaped with 3-d-printed molds to design flexible and conformal antennas. *IEEE Transactions on Antennas and Propagation*, 68(6):4967–4972, 2020. doi: 10.1109/TAP.2020.2969748.

[13] Teng Zheng, Marcin Runowski, I. Martin, K. Soler-Carracedo, Liang Peng, Małgorzata Skwierczyńska, Małgorzata Sójka, Justyna Barzowska, Sebastian Mahlik, Hanoch Hemmerich, Fernando Rivera-López, Kulpinski Piotr, Víctor Lavín, Daniel Alonso, and Dengfeng Peng. Mechanoluminescence and photoluminescence heterojunction for superior multi-mode sensing platform of friction, force, pressure and temperature in fibers and 3d-printed polymers. *Advanced Materials*, 35, 08 2023. doi: 10.1002/adma.202304140.

[14] Christian Hernández-Álvarez, Pablo I. Martín-Hernández, Inocencio R. Martín, Fernando Rivera-López, Hanoch Hemmerich, Maciej Grzegorczyk, Sebastian Mahlik, and Marcin Runowski. Optical temperature sensor evaluation in a working gear motor: Application of luminescence thermometry in industrial technology. *Advanced Optical Materials*, 12(17):2303328, 2024. doi: https://doi.org/10.1002/adom.202303328. URL https://onlinelibrary.wiley.com/doi/abs/10.1002/adom.202303328.

[15] M. A. Hernández-Rodriguez, A. D. Lozano-Gorrín, V. Lavín, U. R. Rodríguez-Mendoza, I. R. Martín, and F. J. Manjón. Analysis of the upconversion emission of yttrium orthoaluminate nano-perovskite co-doped with er3+/yb3+ ions for thermal sensing applications. *Journal of Luminescence*, 202:316–321, 10 2018. ISSN 00222313. doi: 10.1016/j.jlumin.2018.05.078.

[16] Antonio Benayas, Blanca del Rosal, Alberto Pérez-Delgado, Karla Santacruz-Gómez, Daniel Jaque, Gustavo Alonso Hirata, and Fiorenzo Vetrone. Nd:yag near-infrared luminescent nanothermometers. *Advanced Optical Materials*, 3(5):687–694, 2015. doi: https://doi.org/10.1002/adom.201400484. URL https://onlinelibrary.wiley.com/doi/abs/10.1002/adom.201400484.

[17] Elisa Carrasco, Blanca del Rosal, Francisco Sanz-Rodríguez, Ángeles Juarranz de la Fuente, Patricia Haro Gonzalez, Ueslen Rocha, Kagola Upendra Kumar, Carlos Jacinto, and Daniel Solé, José García and Jaque. Intratumoral thermal reading during

photo-thermal therapy by multifunctional fluorescent nanoparticles. *Advanced Functional Materials*, 25(4):615–626, 2015. doi: https://doi.org/10.1002/adfm.201403653. URL https://onlinelibrary.wiley.com/doi/abs/10.1002/adfm.201403653.

[18] Cerón, Elizabeth Navarro, Dirk H. Ortgies, Blanca del Rosal, Fuqiang Ren, Antonio Benayas, Fiorenzo Vetrone, Dongling Ma, Francisco Sanz-Rodríguez, José García Solé, Daniel Jaque, and Emma Martín Rodríguez. Hybrid nanostructures for high-sensitivity luminescence nanothermometry in the second biological window. *Advanced Materials*, 27(32):4781–4787, 2015. doi: https://doi.org/10.1002/adma.201501014. URL https://onlinelibrary.wiley.com/doi/abs/10.1002/adma.201501014.

[19] M. Łukaszewicz, B. Klimesz, A. Szmalenberg, M. Ptak, and R. Lisiecki. Neodymium-doped germanotellurite glasses for laser materials and temperature sensing. *Journal of Alloys and Compounds*, 860:157923, 2021. ISSN 0925-8388. doi: https://doi.org/10.1016/j.jallcom.2020.157923. URL https://www.sciencedirect.com/science/article/pii/S0925838820342870.

[20] Sheila Baker, Thomas Mccleskey, and Gary Baker, editors. *An Ionic Liquid-Based Optical Thermometer*, volume 902. ACS Symposium Series, 03 2005. ISBN 0-8412-3894-4. doi: 10.1021/bk-2005-0902.ch014.

[21] Cid B de Araújo, Glauco S Maciel, Leonardo de S Menezes, Nikifor Rakov, Edilson L Falcão-Filho, Vladimir A Jerez, and Younes Messaddeq. Frequency upconversion in rare-earth doped fluoroindate glasses. *Comptes Rendus Chimie*, 5(12):885–898, 2002. ISSN 1631-0748. doi: https://doi.org/10.1016/S1631-0748(02)01460-1. URL https://www.sciencedirect.com/science/article/pii/S1631074802014601.

[22] Vikas Dubey, Neha Dubey, Marta Michalska Domańska, M. Jayasimhadri, and Sanjay J. Dhoble, editors. *12 - Rare-earth-activated phosphors for energy-efficient solar cell*. Elsevier, 2022. ISBN 978-0-323-89856-0. doi: https://doi.org/10.1016/B978-0-323-89856-0.00011-0. URL https://www.sciencedirect.com/science/article/pii/B9780323898560000110.

[23] W.A. Clarkson. Thermal effects and their mitigation in end-pumped solid-state lasers. *Journal of Physics D: Applied Physics*, 34:2381, 08 2001. doi: 10.1088/0022-3727/34/16/302.

[24] Nan Wang, Zuoling Fu, Yanling Wei, and Tianqi Sheng. Investigation for the upconversion luminescence and temperature sensing mechanism based on bipo4: Yb3+, re3+ (re3+ = ho3+, er3+ and tm3+). *Journal of Alloys and Compounds*, 772, 09 2018. doi: 10.1016/j.jallcom.2018.09.070.

[25] Xinxu Li, Bingting Bao, Xinyu He, Guoqiang Wang, Yantang Huang, Lingyun Li, and Yan Yu. Optical temperature sensing with an er3+, yb3+ co-doped labmoo6

single crystal. *J. Mater. Chem. C*, 11:2494–2504, 2023. doi: 10.1039/D2TC04784E. URL http://dx.doi.org/10.1039/D2TC04784E.

[26] Yong Qiang Wang, Xingbang Dong, Huanjun Zhang, Xiaobo Deng, and Xuerui Cheng. Upconversion luminescence, laser heating effect and temperature sensing properties of β-binbo4:er3+/yb3+. *Journal of Electronic Materials*, 50, 11 2020. doi: 10.1007/s11664-020-08584-y.

[27] Jia Zhang and Chen Jin. Electronic structure, upconversion luminescence and optical temperature sensing behavior of yb3+-er3+/ho3+ doped nalamgwo6. *Journal of Alloys and Compounds*, 783:84–94, 2019. ISSN 0925-8388. doi: https://doi.org/10.1016/j.jallcom.2018.12.281. URL https://www.sciencedirect.com/science/article/pii/S0925838818348394.

[28] Franzette Paz-Buclatin, Fernando Rivera-López, Oswaldo González, Inocencio R. Martín, Leopoldo L. Martin, and Dragana J. Jovanović. Gdvo4:er3+/yb3+ nanocrystalline powder as fluorescence temperature sensor. application to monitor the temperature of an electrical component. *Sensors and Actuators A: Physical*, 299:111628, 2019. ISSN 0924-4247. doi: https://doi.org/10.1016/j.sna.2019.111628. URL https://www.sciencedirect.com/science/article/pii/S0924424719312397.

[29] Ranjana Trivedi, Geetika Mathur, and Ashish Mathur. A survey on platinum temperature sensor. *International Journal of Soft Computing and Engineering*, 1, 2011.

[30] J Martin Bland and DouglasG Altman. Statistical methods for assessing agreement between two methods of clinical measurement. *The lancet*, 327(8476):307–310, 1986.

[31] Engineering Medicine, National Academies of Sciences Engineering, Medicine, et al. Replicability. *Reproducibility and Replicability in Science*, 2019.

[32] Barry N Taylor, Chris E Kuyatt, et al. *Guidelines for evaluating and expressing the uncertainty of NIST measurement results*, volume 1297. US Department of Commerce, Technology Administration, National Institute of ..., 1994.